Spectral broadening effects on metal photoemission by femtosecond laser pulses

Hervé Jouin* and Guillaume Duchateau
Centre Lasers Intenses et Applications, UMR No. 5107, Université de Bordeaux, CNRS, CEA, 33405 Talence, France

(Received 19 December 2018; published 24 January 2019)

Emitted electronic densities from an Al surface have been computed for various temporal shapes of near-infrared femtosecond laser pulses (less than or equal to 20 fs) over a wide range of low and intermediate laser intensities. At low intensities photoemission originates from the high-energy tail of the pulse spectrum leading to linear absorption in all cases, even if several photons are necessary to eject an electron at higher intensities. We propose an analytical method to calculate the transition intensity in which the behavior of emitted densities evolves from the single-photon I_m slope to the multiphoton I_m^n one (with I_m the maximum intensity and n the number of absorbed photons). We show that the use of a flat-top profile or at least of a super-Gaussian envelope enables strong electron emission at very low intensities for realistic pulse durations and should allow experimental observation of the transition between these two regimes of photoemission.

DOI: 10.1103/PhysRevA.99.013433

I. INTRODUCTION

In recent years, femtosecond pulse temporal shaping has attracted considerable interest for numerous applications as light-wave communications or coherent control of quantum nonlinear processes (see [1] and references therein). Among the various techniques developed to achieve waveform synthesis, one can distinguish the use of acousto-optic programmable dispersive filters [2] or the spatial masking of the spatially dispersed optical frequency spectrum [1]. It is now possible to generate almost arbitrary ultrafast waveforms with control of amplitude, polarization, and phase in the near infrared, visible, and also ultraviolet spectral ranges [3]. As the temporal shaping modifies the laser pulse spectrum, it is able to influence the electron dynamics in laser-matter interactions since this dynamics is known to depend on the wavelength. However, up to now only a few works [4,5] have reported on broad spectra femtosecond laser pulse effects on electron dynamics in such a way that an in-depth study of possible significant effects is still lacking.

For this reason, we investigate in this work the influence of the laser pulse shaping, i.e., the pulse spectrum, on the electron photoemission from metal surfaces. Electron densities emitted during the interaction between short (from 5 to 20 fs) near infrared (800 nm) laser pulses with various temporal waveforms and an Al surface have been computed. This metal has been chosen for the simplicity of its electronic structure. Five waveforms are taken into account: a $\cos^2$ temporal profile since it is frequently used in theoretical works, the widespread Gaussian envelope, two super-Gaussian profiles, and also a flat-top envelope as the high-order limit of the super-Gaussian waveforms. Calculations have been performed for the extended domain of low and intermediate fluences ranging from 10^{-8} to 2×10^{-2} J/cm^2, which corresponds roughly to a peak intensity region between 5×10^5 and 10^{12} W/cm^2. For small enough fluences, electron transitions are mainly driven by the high-energy part of the laser spectrum, leading to a linear absorption departing from the standard multiphoton absorption [6,7]. Atomic units are used throughout unless otherwise stated.

II. MODEL

Since the free-electron-gas model closely describes the aluminum electronic structure [8], we represent the metal by means of the jellium model, in which the metal potential reads $V_M(z) = -V_c\Theta(-z)$, with $V_c = E_F + W$, where $E_F = 11.7$ eV is the Fermi energy, $W = 4.26$ eV is the work function of Al(111) [9], z is the electronic coordinate perpendicular to the surface, and Θ is the Heaviside step function. The ejected electron density is evaluated with the expression

$$\varrho_e = \frac{2}{(2\pi)^3}\int d\mathbf{k}_f \int d\mathbf{k}_i \frac{|\mathcal{T}_{if}(k_{iz},k_{fz})|^2\delta(\mathbf{k}_{fs}-\mathbf{k}_{is})}{1+\exp\left[\frac{1}{k_BT}\left(\frac{k_i^2}{2}-\mu\right)\right]}, \quad (1)$$

where the denominator originates from the Fermi-Dirac distribution with k_BT the thermal energy. Due to the short-pulse durations and the modest intensities considered, we have disregarded thermal effects on photoemission and have set $T = 300$ K in all the calculations. For this reason, the chemical potential μ is calculated by means of the first terms of its low-temperature expansion $\mu \simeq E_F - (\pi k_BT)^2/12E_F - \cdots$ [10]. In Eq. (1), the numerator term $|\mathcal{T}_{if}(k_{iz},k_{fz})|^2\delta(\mathbf{k}_{fs}-\mathbf{k}_{is})$ stands for the inelastic transition probability to eject an electron initially within the conduction band with momentum $\mathbf{k}_i(\mathbf{k}_{is},k_{iz})$ towards the metal continuum with final momentum $\mathbf{k}_f(\mathbf{k}_{fs},k_{fz})$, where the subscripts s and z indicate the momentum components parallel and perpendicular to the surface, respectively. The Dirac δ function accounts for the momentum conservation in the plane parallel to the surface due to the fact that the laser field considered here is linearly polarized along the z direction, which results in

*Corresponding author: herve.jouin@u-bordeaux.fr

the translational invariance of the problem along the surface plane. Thus, integrations over k_{ix} and k_{iy} are straightforward and then integrations over k_{fx} and k_{fy} can be performed analytically by considering the angles θ_f and φ_f related to the final momentum in the spherical coordinate system [11]: $dk_{fx}dk_{fy} = k'^2_{fz}d\Omega_f/\cos^3\theta_f$ and $k^2_{fx} + k^2_{fy} = (k'_{fz}\tan\theta_f)^2$, with $k'_{fz} = \sqrt{k^2_{fz} - 2V_c}$. Within this framework, the expression of the emitted density reduces to a double integral (performed numerically by means of Simpson quadratures) over perpendicular components of initial and final momenta. It reads

$$\varrho_e = \frac{k_B T}{2\pi^2}\int_{\sqrt{2V_c}}^{+\infty} dk_{fz}\int_0^{\sqrt{2V_c}} dk_{iz}|\mathcal{T}_{if}(k_{iz},k_{fz})|^2 \times \ln\left\{1+\exp\left(\frac{1}{k_B T}\left[\mu - \frac{k^2_{iz}}{2}\right]\right)\right\}. \quad (2)$$

Due to the low laser intensities and the short-pulse durations considered in this work, the so-called jellium-Volkov wave function is a reliable solution of the time-dependent Schrödinger equation. Within this approach, the transition amplitude reads [12,13]

$$\mathcal{T}_{if} = -i\int_{-\infty}^{+\infty} dt\, F_l(t)\mathcal{G}_{if}(t)\exp\{i[\Delta\varepsilon t + \beta_l(t)]\}, \quad (3)$$

with $\Delta\varepsilon = k^2_{fz}/2 - k^2_{iz}/2$ the perpendicular energy difference between final and initial states, $F_l(t)$ the temporal shape of the laser pulse (with the subscript l standing for the various waveforms used), and $\mathcal{G}_{if}(t)$ a function defined as

$$\mathcal{G}_{if}(t) = \int_{-\infty}^{+\infty} dz\,\Phi^*_{k_{fz}}(\zeta_l(t))z \times \exp\left[\left(i\frac{A_l(t)}{c} + \frac{\Theta(-z)}{\delta_s}\right)z\right]\Phi_{k_{iz}}(z), \quad (4)$$

where $\Phi_{k_{iz}}$ is an outgoing eigenfunction of the jellium Hamiltonian representing an electron of the conduction band and $\Phi_{k_{fz}}$ an incoming eigenfunction describing an electron of the continuum [14]. The vector potential $A_l(t)$, the quiver amplitude $\alpha_l(t)[\zeta_l(t) = z - \alpha_l(t)$ defines the coordinate z shifted by the quiver amplitude], and the ponderomotive energy $\beta_l(t)$ in Eq. (3) are

$$A_l(t) = -c\int_{-\infty}^{t} d\xi\, F_l(\xi),$$
$$\alpha_l(t) = \frac{1}{c}\int_{-\infty}^{t} d\xi\, A_l(\xi),$$
$$\beta_l(t) = \frac{1}{2c^2}\int_{-\infty}^{t} d\xi\, A_l^2(\xi), \quad (5)$$

where c is the speed of light in vacuum. Integrals involved in Eqs. (3) and (5) are performed numerically, whereas the function $\mathcal{G}_{if}(t)$ of Eq. (4) can be expressed analytically due to the simple expressions of jellium eigenfunctions $\Phi_{k_{iz}}$ and $\Phi_{k_{fz}}$. It has been shown [13] that the total field inside the metal (sum of the laser field and the induced one) is very weak for the central laser wavelength considered here ($\lambda_0 = 800$ nm). For this reason, we have allowed the incident field to penetrate into the solid only over the skin depth $\delta_s = \sqrt{\lambda_0\mathcal{R}/\pi\mu_0 c}$, which is of 4.3 nm in the present case since the electrical resistivity of Al at 300 K is $\mathcal{R} = 2.7\times10^{-8}$ Ωm [9].

The temporal waveforms considered read

$$F_l(t) = \mathcal{F}_l E_l(t)\cos(\omega_0 t + \phi_0), \quad (6)$$

where $\mathcal{F}_l$ represents the maximum field strength, ω_0 and ϕ_0 are the carrier frequency and the carrier envelope phase, respectively, and $E_l(t)$ stands for the envelopes in which τ is the pulse duration (i.e., the full width at half maximum) in all cases,

$$E_q(t) = \exp\left(-\ln 2\left[\frac{2t}{\tau}\right]^{2q}\right), \quad (7a)$$
$$E_w(t) = \Pi_{-\tau/2,+\tau/2}(t), \quad (7b)$$
$$E_C(t) = \cos^2\left(\frac{\pi t}{2\tau}\right)\Pi_{-\tau,+\tau}(t), \quad (7c)$$

where q in Eq. (7a) is a nonzero positive integer: $q = 1$ corresponds to the standard Gaussian shape and $q \geqslant 2$ to a super-Gaussian form (cases $q = 3$ and $q = 5$ are considered in this work). In Eqs. (7b) and (7c), $\Pi_{t_1,t_2}(t) = \Theta(t - t_1) - \Theta(t - t_2)$ is the window function, in such a way that the flat-top waveform $E_w(t)$ is the limit of $E_q(t)$ for $q \to +\infty$. Furthermore, to compare the influence of the various waveforms, the maximum field strength $\mathcal{F}_l$ of Eq. (6) is obtained through the normalization

$$\int_{-\infty}^{+\infty} dt\, F_l^2(t) = \frac{8\pi}{c}J_0 \equiv \int_{-\infty}^{+\infty} d\omega|\mathcal{F}_l(\omega)|^2, \quad (8)$$

where J_0 is the fluence, $\mathcal{F}_l(\omega)$ is the Fourier transform of the laser field $F_l(t)$, and the second equality of Eq. (8) comes from Parseval's identity. Maximum field strength values $\mathcal{F}_l$ obtained from this normalization procedure substantially vary with the shape of the laser pulse in the range of pulse durations studied here.

III. RESULTS

Emitted densities computed for the five previous waveforms are displayed in Fig. 1 for $\tau = 20$ fs and $\phi_0 = \pi/2$. This value of the carrier envelope phase has been used throughout, although calculations (not reported) considering other values have been performed. For the smaller pulse duration considered after (5 fs), emitted densities as well as transition intensities (discussed below) substantially vary with the carrier envelope phase, while these variations decrease with increasing pulse duration. However, the choice of the particular $\phi_0 = \pi/2$ value for our illustrations does not affect the generality of our conclusions.

As the spectrum of a near infrared 800-nm laser pulse is centered around 1.55 eV and since the work function of Al(111) is 4.26 eV, at least three photons are necessary to eject an electron from the conduction band. Consequently, within the multiphoton fluence range, emitted densities follow a J_0^3 power law. This is exactly what can be observed in Fig. 1 in the case of Gaussian, super-Gaussian, and $\cos^2$ waveforms for fluences greater than 10^{-5} J/cm^2, which corresponds to a maximum intensity around 10^9 W/cm^2. At lower fluences, the variation of emitted densities corresponding to these four

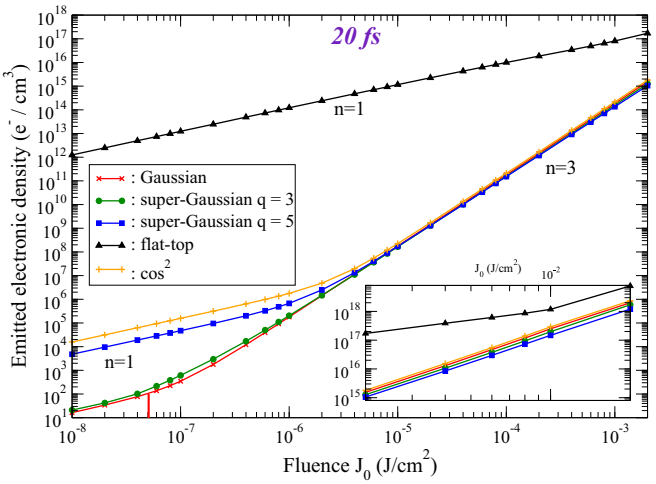

FIG. 1. Emitted electronic densities ϱ_e (in e^-/cm^3) as a function of the fluence J_0 (in $\mathrm{J/cm}^2$) for $\omega_0 = 0.057$ ($\lambda_0 = 800$ nm), $\phi_0 = \pi/2$, and $\tau = 20$ fs: Gaussian shape, red line with $\times$; $q = 3$ super-Gaussian waveform, green line with $\bullet$; $q = 5$ super-Gaussian envelope, blue line with $\blacksquare$; flat-top form, black line with $\blacktriangle$; and $\cos^2$ shape, orange line with $+$. The vertical red line indicates the transition fluence (see the text) for the Gaussian shape. The inset shows the emitted densities in the higher-fluence region ranging from 2×10^{-3} to 2×10^{-2} $\mathrm{J/cm}^2$.

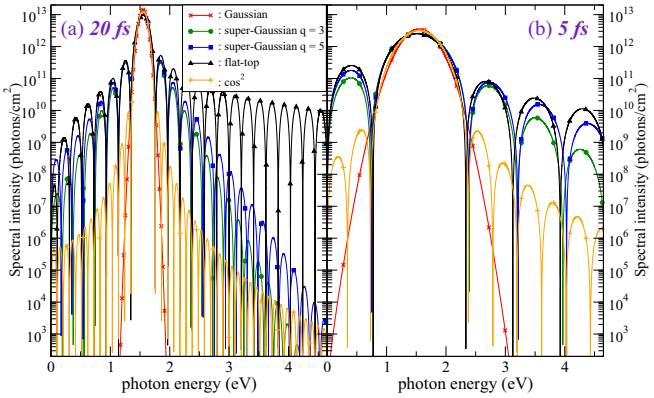

FIG. 2. Spectral intensity (in photons/cm^2) as a function of photon energy (in eV) for $\omega_0 = 0.057$ ($\hbar\omega_0 = 1.55$ eV), $\phi_0 = \pi/2$, $J_0 = 10^{-7}$ $\mathrm{J/cm}^2$, and (a) $\tau = 20$ fs or (b) $\tau = 5$ fs: Gaussian shape, red line with $\times$; $q = 3$ super-Gaussian waveform, green line with $\bullet$; $q = 5$ super-Gaussian envelope, blue line with $\blacksquare$; flat-top form, black line with $\blacktriangle$; and $\cos^2$ shape, orange line with $+$.

profiles departs from the J_0^3 law to reach a J_0 behavior at very low fluences. As demonstrated below, this behavior originates from the high-energy tail of the pulse spectrum and corresponds to electron emission through the absorption of only one photon whose energy is at least the work function value. Transition intensities $\mathcal{I}_{\mathrm{tr}}$ from the $n = 1$ to the $n = 3$ absorption behaviors are around 10^7 $\mathrm{W/cm}^2$ (5×10^{-8} $\mathrm{J/cm}^2$) for the Gaussian shape as well as for the $q = 3$ super-Gaussian one (whose emitted densities are very close in the whole range of fluences considered) and around 2×10^8 $\mathrm{W/cm}^2$ (10^{-6} $\mathrm{J/cm}^2$) and 4×10^8 $\mathrm{W/cm}^2$ (2×10^{-6} $\mathrm{J/cm}^2$) for the $q = 5$ super-Gaussian profile and the $\cos^2$ one, respectively. In the case of the flat-top profile, ejected densities are much more important for all considered fluences and also follow a J_0 power law up to 10^{-2} $\mathrm{J/cm}^2$ ($I_m \approx 10^{12}$ $\mathrm{W/cm}^2$; see the inset of Fig. 1).

We will see below that in the low-fluence single-photon absorption regime, emitted densities are proportional to $|\mathcal{F}_l(\omega)|^2$ of Eq. (8), i.e., to the spectral intensities corresponding to the various waveforms studied in this work, which are displayed in Fig. 2 as a function of the photon energy. Hence, the relative strength of electronic emission at low fluences related to the five waveforms, displayed in Fig. 1 for 20 fs, are explained by the amplitude of the corresponding spectral intensities depicted in Fig. 2(a) for photon energies greater than 4.26 eV. One can see in Fig. 2(a) that spectral intensities in this photon energy range are very weak with respect to the main peak magnitude, except for the flat-top profile whose spectral intensity dominates by several orders of magnitude those corresponding to the four other shapes. Moreover, the spectral intensity corresponding to the $\cos^2$ shape (which decreases as ω^{-1} far from the central peak) is higher than those related to the super-Gaussian and Gaussian profiles whose decrease is exponential in this spectral range. Consequently, one understands the magnitude of emitted densities in the single-photon absorption regime as a function of the temporal profile, which is, for increasing values (see Fig. 1), Gaussian, $q = 3$ super-Gaussian, $q = 5$ super-Gaussian, $\cos^2$, and the flat-top shape that dominates.

One observes in Fig. 2(b) that the magnitude of the spectral intensity (for $\hbar\omega \geqslant 4.26$ eV) related to the flat-top profile for 5-fs pulse duration is similar to the one of Fig. 2(a) in the 20-fs case, while those corresponding to super-Gaussian shapes are strongly increased in such a way that the values corresponding to the $q = 5$ super-Gaussian envelope are close to those of the flat-top profile. To a lesser extent, spectral intensities related to the $\cos^2$ shape and to the Gaussian one are also increased with respect to the 20-fs case.

Consequently, emitted densities for 5-fs pulse duration, which are reported in Fig. 3, are greater than their 20-fs counterparts, except for the flat-top profile whose corresponding emitted densities are close in both cases. For 5-fs pulse duration, the magnitude of emitted densities in the single-photon-absorption regime as a function of the temporal profile is, for increasing values, Gaussian, $\cos^2$, $q = 3$ super-Gaussian, $q = 5$ super-Gaussian, and flat-top. Calculations similar to those presented in Figs. 1 and 3 have been performed also for a 10-fs pulse duration (results not reported for the sake of conciseness) and show intermediate behaviors between the 20- and 5-fs cases. In all cases, the emitted density related to the Gaussian shape presents the lower values in the single-photon regime while the greater ones are obtained by consideration of the flat-top envelope, which is also the shape for which the single-photon absorption is conserved for the wider domain of fluences. Moreover, one can note in Fig. 3 that transition intensities from the single-photon to the multiphoton regimes are greater than in the 20-fs case: around 10^8 $\mathrm{W/cm}^2$ for the Gaussian shape, 1.5×10^{10} $\mathrm{W/cm}^2$ for the $\cos^2$ envelope, around 2×10^{11} $\mathrm{W/cm}^2$ for the $q = 3$ super-Gaussian profile, and 4×10^{11} $\mathrm{W/cm}^2$ for the $q = 5$ super-Gaussian and flat-top waveforms. Furthermore, the structures appearing in the emitted densities at high fluences for the flat-top and $q = 5$

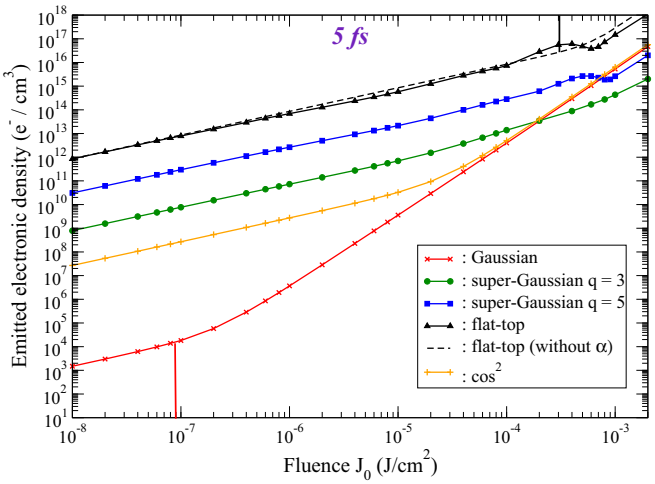

FIG. 3. Same as Fig. 1 for $\tau = 5$ fs. The dashed black line corresponds to the flat-top profile without consideration of $\alpha_w(t)$ in the calculation (see the text). The vertical red and black lines indicate the transition fluences (see the text) for the Gaussian shape and the flat-top profile, respectively.

super-Gaussian profiles in the 5-fs case are due to the quiver amplitude $\alpha_l(t)$ [see Eqs. (4) and (5)]. Indeed, these structures disappear if one neglects the quiver amplitude, as it can be seen in Fig. 3 for the flat-top case (dashed black line). Calculations without $\alpha_l(t)$ have been performed for all the waveforms considered here and we have observed that the influence of this factor on emitted densities is negligible in the single-photon fluence region, while it produces a decrease of a factor around 2 in the multiphoton region. We have also observed that the ponderomotive energy $\beta_l(t)$ does not play any significant role on ejected densities in the domain of fluence under consideration.

For practical reasons, the $\cos^2$ waveform is frequently used in theoretical works in place of the Gaussian shape. One can see in Figs. 1 and 3 that these envelopes lead to the same emitted densities at high enough fluences. However, in the low-fluence range emitted densities obtained by consideration of the $\cos^2$ shape are significantly greater than those related to the Gaussian form and these differences increase with decreasing pulse duration. This is due to the fact that the high-energy tail of the $\cos^2$ spectral intensity is much more important than the Gaussian one (see Fig. 2).

IV. TRANSITION INTENSITY

In order to determine the intensity $\mathcal{I}_{\rm tr}$ for which the behavior of ejected densities evolves from the single-photon I_m power law to the multiphoton I_m^n one, we have expanded the term $\exp[iA_l(t)z/c]$ of Eq. (4) in a Taylor series and we have also neglected the quantities $\alpha_l(t)$ and $\beta_l(t)$. After a straightforward analysis based on Eqs. (2)–(5), emitted densities can be expressed as

$$\varrho_e = \sum_{p=0}^{+\infty} \eta_p \, I_m^{p/2+1}, \tag{9}$$

in which the coefficients η_p vanish for odd values of p. Indeed, it can be shown that these coefficients contain products of integrals over time (discussed below) in which different resonance conditions appear related to energy conservation like $(\Delta\varepsilon - \omega_0)^{-1}$ and $(\Delta\varepsilon - 2\omega_0)^{-1}$. Since the two resonance conditions cannot be fulfilled simultaneously, one of these integrals vanishes. This fact has also been verified numerically. Then ϱ_e can be expanded as

$$\varrho_e = \sum_{n=1}^{+\infty} \sigma_n I_m^n = \sigma_1 I_m + \sigma_2 I_m^2 + \sigma_3 I_m^3 + \cdots, \tag{10}$$

where n is the multiphotonic order and the weights σ_n read

$$\sigma_n = \frac{k_B T}{2\pi^2}\left[\frac{8\pi}{c}\right]^n \int_{\sqrt{2V_c}}^{+\infty} dk_{fz} \int_0^{\sqrt{2V_c}} dk_{iz} \left\{ \sum_{j=0}^{2n-2} C_j \, C_{2n-j-2}^* \right\}$$
$$\times \ln\left\{1 + \exp\left(\frac{1}{k_B T}\left[\mu - \frac{k_{iz}^2}{2}\right]\right)\right\}, \tag{11}$$

in which the coefficients $C_m(k_{iz}, k_{fz})$ come from the expansion of $|\mathcal{T}_{if}(k_{iz}, k_{fz})|^2$ and are given by

$$C_m(k_{iz}, k_{fz}) = \frac{i^{m+1}}{m!} \mathcal{M}_m(k_{iz}, k_{fz}) \mathcal{L}_m(k_{iz}, k_{fz}), \tag{12}$$

with

$$\mathcal{M}_m = \int_{-\infty}^{+\infty} dz \, \Phi_{k_{fz}}^*(z) z^{m+1} \exp\left(\frac{\Theta(-z)z}{\delta_s}\right) \Phi_{k_{iz}}(z),$$
$$\mathcal{L}_m = \int_{-\infty}^{+\infty} dt \, f_l(t) a_l^m(t) \exp(i\Delta\varepsilon t), \tag{13}$$

where $f_l(t) = F_l(t)/F_l$ is the normalized temporal shape and $a_l(t) = -\int_{-\infty}^{t} d\xi \, f_l(\xi)$ is the normalized vector potential. One can note in Eq. (13) that the matrix element $\mathcal{M}_m$ is characteristic of the metal target, while $\mathcal{L}_m$ is mainly characteristic of the laser pulse. Furthermore, in the case of the coefficient σ_1 of Eq. (10), the discrete sum in Eq. (11) reduces to $|C_0|^2 = |\mathcal{M}_0\mathcal{L}_0|^2$, where $\mathcal{M}_0$ is the dipole matrix element and $\mathcal{L}_0$ the Fourier transform of the normalized temporal profile with $\Delta\varepsilon$ the difference in perpendicular energy between the final and the initial state. The term $|\mathcal{L}_0|^2$ in the σ_1 coefficient is responsible for the variations of the emitted densities as a function of the pulse waveform in the single-photon absorption regime that can be observed in Figs. 1 and 3.

Then we define the transition intensity as the intensity for which the sum of the terms from $n = 2$ to $n + 1$ of Eq. (10) overtake the first one. Thus this value is obtained through

$$\sum_{j=2}^{n+1} \sigma_j \mathcal{I}_{\rm tr}^j = \sigma_1 \mathcal{I}_{\rm tr}. \tag{14}$$

This amounts to finding the root with physical meaning of an nth degree polynomial. The sum up to $n + 1$ in Eq. (14) is necessary in the case of a smooth transition as for the flat-top profile or for the 5-fs super-Gaussian envelope; otherwise a sum up to n is enough. In the case at hand with $n = 3$, this method leads, for example, to 9×10^{-8} and 5×10^{-8} J/cm^2 for the transition fluence in the cases of 5- and 20-fs Gaussian shapes, respectively, and 3×10^{-4} J/cm^2 in the 5-fs flat-top

case. These values, which are in agreement with what can be observed in Figs. 1 and 3, are indicated by vertical lines in these figures.

In the 20-fs case (Fig. 1), emitted densities in the fluence transition regions for the Gaussian, super-Gaussian, and $\cos^2$ waveforms appear too weak to allow the experimental observation of the transition between the two photoemission regimes. This is probably also the case for Gaussian and $\cos^2$ profiles at 5 fs (Fig. 3). However, such a detection should be possible by consideration of a flat-top envelope (emitted densities around 10^{17} e^-/cm^3 in the transition region) or by means of a super-Gaussian profile at short-pulse duration.

Finally, it must be noted that the jellium model used in this work to represent the simple electronic structure of aluminum is not able to account for localized surface states like intrinsic surface states or image potential states [15]. It has been shown [13,16] that these partially occupied states which display a highly localized electron density at the edge of the crystal surface can significantly influence the photoemission process. Consequently, localized surface states whose corresponding eigenfunctions and eigenenergies would appear in Eq. (13) can modify the transition intensity value. However, the study of this effect is beyond the scope of the present work.

V. SUMMARY

We have evaluated electronic densities emitted from an Al(111) surface irradiated by near infrared femtosecond (less than 20 fs) laser pulses with various temporal profiles over a large range of intensities. Even if several photons are necessary to eject an electron in the intermediate multiphoton intensity range, ionization takes place through the absorption of only one photon at low enough intensities. This behavior has been shown to originate from the high-energy part of the pulse spectrum. Consequently, our attention has been attracted by the intensity region in which the behavior of ejected densities evolves from the single-photon absorption I_m power law to the I_m^n multiphotonic law (with $n = 3$ in the present case). An analytical method is proposed to calculate the transition intensity $\mathcal{I}_{\mathrm{tr}}$ between these two regimes of photoemission. Our study shows that the use of a flat-top profile or at least a super-Gaussian one allows us to obtain important emission at very low intensities with realistic laser pulses durations.

The transition evidenced here results only from the energy conservation associated with various parts of the pulse spectrum, the present conclusions are expected to be universal, taking place for all types of targets (atoms, molecules, and solids). To our knowledge, such a transition has not been evidenced experimentally up to now. In the case of gaseous targets, emitted electronic densities at low intensities are probably too weak even with short shaped pulses to enable such measurement. Solids and in particular metals are good candidates due to the high electronic densities involved leading to relatively large emitted densities of 10^{16}–10^{17} e^-/cm^3 where the linear-nonlinear transition takes place.

ACKNOWLEDGMENT

The authors would like to thank Dr. D. Descamps for useful discussions related to pulse shaping.

[1] A. M. Weiner, Opt. Commun. **284**, 3669 (2011).
[2] F. Verluise, V. Laude, Z. Cheng, C. Spielmann, and P. Tournois, Opt. Lett. **25**, 575 (2000).
[3] E. Hertz, F. Billard, G. Karras, P. Béjot, B. Lavorel, and O. Faucher, Opt. Express **24**, 27702 (2016).
[4] A. Bourgeade and G. Duchateau, Phys. Rev. E **85**, 056403 (2012).
[5] G. Duchateau and A. Bourgeade, Phys. Rev. A **89**, 053837 (2014).
[6] H. Jouin, M. Raynaud, G. Duchateau, G. Geoffroy, A. Sadou, and P. Martin, Phys. Rev. B **89**, 195136 (2014).
[7] N. Fedorov, G. Geoffroy, G. Duchateau, L. Štolcová, J. Proška, F. Novotný, M. Domonkos, H. Jouin, P. Martin, and M. Raynaud, J. Phys: Condens. Matter **28**, 315301 (2016).
[8] Z. Lin, L. V. Zhigilei, and V. Celli, Phys. Rev. B **77**, 075133 (2008).
[9] D. R. Lide, *Handbook of Chemistry and Physics*, 84th ed. (CRC, New York, 2003).
[10] S. Micheau, F. A. Gutierrez, B. Pons, and H. Jouin, J. Phys. B: At. Mol. Opt. Phys. **38**, 3405 (2005).
[11] S. V. Yalunin, M. Gulde, and C. Ropers, Phys. Rev. B **84**, 195426 (2011).
[12] M. N. Faraggi, M. S. Gravielle, and D. M. Mitnik, Phys. Rev. A **76**, 012903 (2007).
[13] C. A. Ríos Rubiano, R. Della Picca, D. M. Mitnik, V. M. Silkin, and M. S. Gravielle, Phys. Rev. A **95**, 033401 (2017).
[14] M. S. Gravielle, Phys. Rev. A **58**, 4622 (1998).
[15] E. V. Chulkov, V. M. Silkin, and P. M. Echenique, Surf. Sci. **437**, 330 (1999).
[16] C. A. R. Rubiano, M. S. Gravielle, D. M. Mitnik, and V. M. Silkin, Phys. Rev. A **85**, 043422 (2012).